Surface plasmon excitation using a Fourier-transform infrared spectrometer: Live cell and bacteria sensing

Vladislav Lirtsman, Michael Golosovsky, and Dan Davidov

Citation: Review of Scientific Instruments **88**, 103105 (2017); doi: 10.1063/1.4997388
View online: http://dx.doi.org/10.1063/1.4997388
View Table of Contents: http://aip.scitation.org/toc/rsi/88/10
Published by the American Institute of Physics

Surface plasmon excitation using a Fourier-transform infrared spectrometer: Live cell and bacteria sensing

Vladislav Lirtsman, Michael Golosovsky,[a] and Dan Davidov
The Racah Institute of Physics, The Hebrew University of Jerusalem, 91904 Jerusalem, Israel

(Received 24 July 2017; accepted 23 September 2017; published online 13 October 2017)

We report an accessory for beam collimation to be used as a plug-in for a conventional Fourier-Transform Infrared (FTIR) spectrometer. The beam collimator makes use of the built-in focusing mirror of the FTIR spectrometer which focuses the infrared beam onto the pinhole mounted in the place usually reserved for the sample. The beam is collimated by a small parabolic mirror and is redirected to the sample by a pair of plane mirrors. The reflected beam is conveyed by another pair of plane mirrors to the built-in detector of the FTIR spectrometer. This accessory is most useful for the surface plasmon excitation. We demonstrate how it can be employed for label-free and real-time sensing of dynamic processes in bacterial and live cell layers. In particular, by measuring the intensity of the CO_2 absorption peak one can assess the cell layer metabolism, while by measuring the position of the surface plasmon resonance one assesses the cell layer morphology. *Published by AIP Publishing.*
https://doi.org/10.1063/1.4997388

I. INTRODUCTION

Infrared spectroscopy is an effective analytical tool for detecting functional chemical groups and for characterization of covalent bonding. Conventional Fourier-Transform Infrared (FTIR) spectrometers use incoherent broadband infrared radiation to measure transmission and reflection spectra of liquid and solid samples in order to find their chemical composition. High sensitivity and possibility to work with small sample volumes are achieved by the operation in the Attenuated Total Internal Reflection (ATR) regime which is based on evanescent rather than propagating infrared wave. Enhanced sensitivity of the ATR technique is derived from the energy concentration in the evanescent field of the surface wave.

In distinction to ATR which is a non-resonant technique, the surface plasmon wave is a resonant phenomenon, and the intensity enhancement in its evanescent field is significantly larger than in the ATR regime. The sensing technologies based on the surface plasmon resonance in the visible range proliferated widely over the last decade. These technologies exploit high energy density in the surface plasmon wave which is translated into incredible sensitivity of the surface-plasmon-based sensors.[1] Based on this success, much effort was spent to push the surface plasmon technology into the infrared range.[2–4] The infrared surface plasmon wave is at the core of emerging methods for label-free and real-time probing of molecules,[2,5–7] organic layers,[8–10] and live cells.[11] It would be especially advantageous to combine the surface plasmon technique and infrared spectroscopy together to achieve highly sensitive spectroscopic measurements. So far, two groups[2,12] succeeded in combining surface plasmon excitation with an FTIR spectrometer, and their efforts resulted in surface-plasmon-based *near-infrared* spectroscopy.

In this study, we make a next step and demonstrate integration of the infrared surface plasmon technique with the FTIR spectrometer to achieve surface-plasmon-based *mid-infrared* spectroscopy. We have recently demonstrated that this mid-infrared Fourier-transform surface plasmon resonance (FT-SPR) technique is very useful for label-free and real-time monitoring of kinetic processes in live cells.[11,13–17] The above studies were performed using a custom optics which fits the purposes of a single research group but cannot be used by the broad research community. It is based on the open path configuration of the FT-SPR setup, and thus its operation is limited by atmospheric absorption. In this work, we demonstrate a compact design of the FT-SPR setup for the mid-infrared range that is fully integrated with a conventional FTIR spectrometer and can be used by any researcher. The compact design eliminates the open-path beam propagation and adds a new functionality—operation under controlled atmosphere.

II. DESIGN CONSIDERATIONS

The combination of infrared spectroscopy with the surface plasmon excitation requires a broadband coupler. Several such couplers have been developed recently, and they include multipath diffraction grating,[18] plasmonic filter array,[7] wide-band plasmonic nanoantenna,[8,9] or specially etched Si substrate.[19] Still, these couplers have limited bandwidth, and the traditional Kretschmann's geometry based on a metal-coated prism[20] remains a preferred setup for broadband surface plasmon excitation. To be used in surface-plasmon-based spectroscopy, this setup requires a well-collimated infrared beam with a variable wavelength. Although such a beam can be produced with quantum-cascade lasers, it is highly desirable to use a standard Fourier-transform infrared spectrometer as a source of broadband infrared radiation. However, there is an obstacle in this way since conventional FTIR spectrometers operate with a convergent beam rather than with a collimated beam, as required for the surface plasmon excitation.

[a]Electronic mail: michael.golosovsky@mail.huji.ac.il

To overcome this obstacle, Frutos *et al.*[2] used the fact that conventional FTIR spectrometers have an auxiliary window for the collimated beam output. Frutos *et al.* built an external SPR accessory using this auxiliary window and a BK-7 glass lens for beam collimation. Their near-infrared FT-SPR accessory has been commercially implemented[21] and successfully used for chemical and biological studies.[10] Its drawback is of relatively high cost since it requires an additional expensive infrared detector.

Menegazzo *et al.*[12,22] aimed at combining the surface plasmon and FTIR techniques in a more economic and compact way. This group designed a FT-SPR accessory that fits the sample compartment of a standard FTIR spectrometer. The design is based on the Harrick-Seagull ATR accessory to which Menegazzo *et al.*[12] added a BK-7 glass lens for beam collimation and an ingenious motor-driven mechanical system for mirror rotation to achieve variable incident angles. This setup uses the built-in detector of the FTIR spectrometer, and thus it does not require a separate infrared detector. Hence this design has obvious advantages over external accessory of Ref. 21.

Notably, both known FT-SPR accessories[2,12] use a BK-7 glass lens for beam collimation, and this limits their operation to the near-infrared range. In principle, the BK-7 glass lens can be replaced by a ZnS or ZnSe lens to extend the operation of the accessory into the mid-infrared range.[16] In reality, this is prohibitive due to high reflection losses and chromatic aberrations of ZnS and ZnSe lenses that limit their use in mid-infrared spectroscopy.

Recently, we developed an open-path mid-infrared FT-SPR setup where beam collimation is achieved not with lenses but with parabolic off-axis mirrors.[11] Thus, the only non-metallic optical element in our setup is a high-refractive-index prism, as required by Kretschmann's geometry. This setup extends the FT-SPR technique into the mid-infrared range. However, it requires a separate infrared detector and outdoor mechanical and optics design. To make this FT-SPR tool more compact and less expensive, we engineered now a FT-SPR accessory for the mid-IR range that fits the sample compartment of a conventional FTIR spectrometer and eliminates the need in a separate detector. An important technical advantage of this compact accessory is the possibility to work under a controlled atmosphere. We demonstrate here this accessory and its use for label-free monitoring of kinetic processes in live cells and bacteria.

III. TECHNICAL DESCRIPTION OF THE FT-SPR ACCESSORY

Conventional FTIR spectrometers operate with a convergent unpolarized infrared beam that enters the sample compartment through the entrance window, passes through the sample mounted in the focus of the beam, leaves the sample compartment through the exit window, and then goes to the built-in infrared detector. Our idea is to use the built-in focusing mirror of the FTIR spectrometer as a part of a beam collimator. This collimator is mandatory for effective surface plasmon excitation. Figure 1 shows our design. An off-axis parabolic mirror P1 is mounted in the center of the sample compartment,

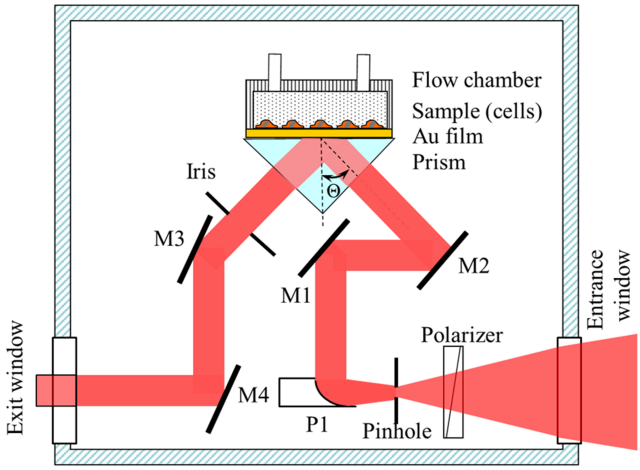

FIG. 1. An accessory for beam collimation in the FTIR spectrometer. The converging infrared beam enters the sample compartment through the entrance window and passes through the pinhole mounted at the point of beam's convergence. An off-axis parabolic mirror P1 is mounted in the confocal position with respect to the built-in focusing mirror of the FTIR spectrometer in such a way that the output beam is collimated. The collimated beam propagates at 90° to the optical axis of the incident beam and is directed to the sample by a pair of plane metallic mirrors M1 and M2. The reflected beam passes through a variable iris and is deflected by plane mirrors M3 and M4 that make it collinear with the optical axis of the incident beam. The mirrors M1 and M2 bring the beam out of the horizontal plane to the vertical plane, while the mirrors M3 and M4 bring it back to the horizontal plane. To polarize the beam (this is mandatory for the surface plasmon excitation), a wire-grid polarizer is mounted in front of the pinhole.

in such a way that this mirror is in the confocal position with respect to the built-in focusing mirror of the FTIR spectrometer. Thus, we achieved collimation of the infrared convergent beam that enters the sample compartment. To allow surface plasmon measurements, we also introduced a metal wire-grid polarizer in the path of the incident beam. For better collimation, we introduced a pinhole at the point of beam convergence. The collimated beam diameter is determined by the ratio of the focal lengths of two mirrors and by their diameters. The collimated beam is further deflected by two plane mirrors M1 and M2 onto the sample. To block scattered light, one can introduce a variable iris mounted close to the sample on the path of either incident or reflected beams. The reflected beam is deflected by a pair of plane mirrors M3 and M4 that make it collinear with the optical axis of the incident beam, in such a way that the reflected beam goes into the built-in detector of the FTIR spectrometer as if its source were the center of the entrance window. Note that the direction of the beam reflected from the sample and the direction of the beam passing through the exit window do not intersect. Although transition from one such skew beam to another is usually done with three plane mirrors, we have to do this with two plane mirrors due to space limitations.

We used the removable base plate of the FTIR spectrometer as an optical breadboard. Our specially designed sample holder is also attached to this base plate. It can be staffed with a flat sample for reflectivity measurements, with a prism with an overlaid sample for ATR measurements or with a metal-coated prism with an overlaid sample for SPR measurements. The whole accessory including the sample holder can be aligned

inside the FTIR spectrometer or can be pre-aligned outside and then inserted into the sample compartment. Having in mind liquids and biological samples such as live cell layers, we designed our accessory in such a way that the prism base is horizontal. (The design for the sample in the vertical position is even simpler since in this configuration all beams propagate in one plane.) Our accessory allows spectroscopic measurements at a fixed angle of incidence. This angle can be varied in narrow limits by manually adjusting the height of the prism-sample assembly and by rotating the M2, M3, and M4 mirrors.

Figures 2 and 3 show a specific implementation of this FT-SPR accessory for measurements with horizontally oriented samples attached to the prism in Kretschmann's geometry. We used a right-angle ZnS or sapphire prism coated with a 12–18 nm thick Au layer. To ensure multiple use of the Au-coated prism, we deposited on it a thin dielectric overlayer (MgO, PMMA, etc.). While a thick dielectric overlayer introduces unwanted waveguide resonances, a very thin overlayer with the thickness of tens of nanometers does not qualitatively change the infrared reflectivity spectra—it only slightly shifts the wavelength of the reflectivity minimum corresponding to the surface plasmon resonance. Moreover, a thin dielectric overlayer between the prism and the sample brings an additional advantage—it increases sensitivity of the surface plasmon sensor.[23]

The sample is deposited on the Au-coated prism. To operate with liquids and for live cell studies, we designed a special flow chamber (Fig. 4) with temperature stabilization in the range from 5 °C to 60 °C and an accuracy of 0.1 °C.[24] The prism is a part of this flow chamber. The live cells or bacteria are grown directly on the prism or are injected into the flow chamber in the course of experiment. The flow chamber is filled with a buffer medium whose flow rate can be varied. The surface plasmon senses the cell/bacterial layer from below. The flow chamber has a transparent window to allow simultaneous optical microscopy inspection from above.

The principle of operation of this accessory is captured by Eq. (1) which is a resonant condition for the surface plasmon excitation using a metal-coated prism in Kretschmann's geometry,

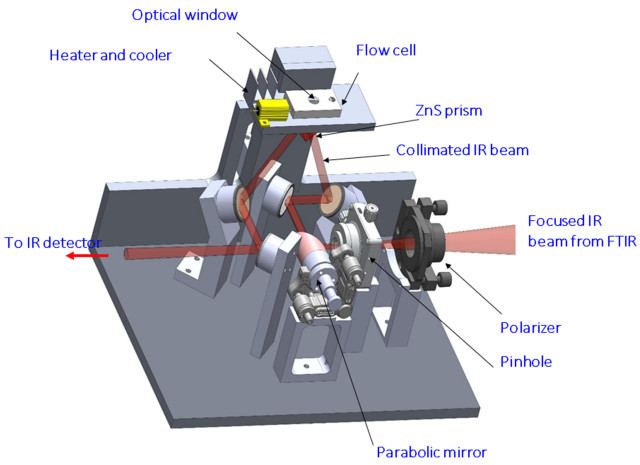

FIG. 2. Computer-aided draft (CAD) of the FT-SPR accessory.

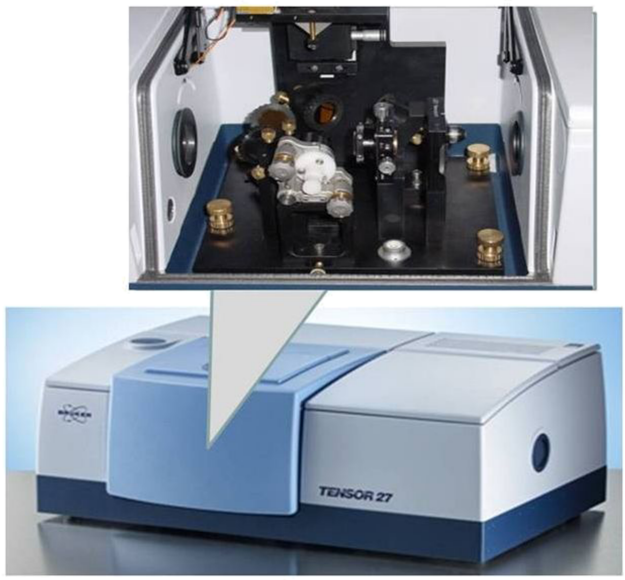

FIG. 3. The FT-SPR accessory in the sample compartment of the Bruker Equinox 55 FTIR spectrometer.

$$n_{prism}\sin\theta = Re\left[\left(\frac{\varepsilon_m\varepsilon_d}{\varepsilon_m+\varepsilon_d}\right)^{1/2}\right], \quad (1)$$

where n_{prism} is the refractive index of the prism, θ is the angle of incidence, ε_d and ε_m are the complex dielectric permittivities of the dielectric and of the metal, correspondingly. The value of interest is the refractive index of the dielectric, $n_d = \sqrt{\varepsilon_d}$. Since n_{prism}, n_d, and ε_m are wavelength-dependent, the resonant condition captured by Eq. (1) singles out one or

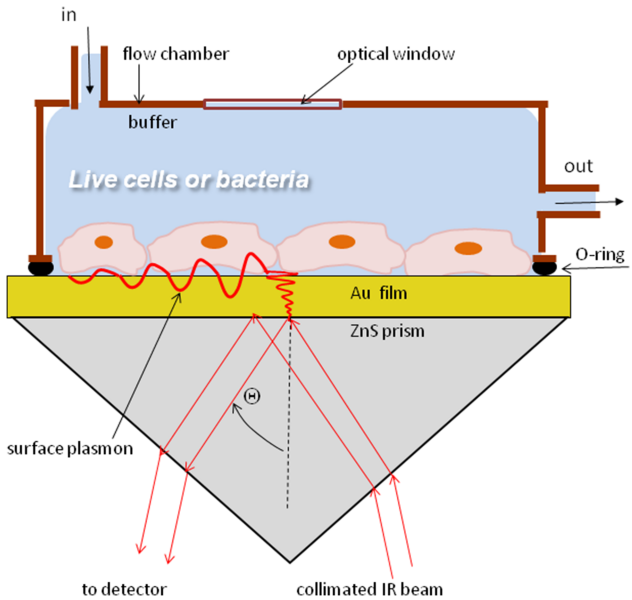

FIG. 4. Sample holder and flow chamber. The sample (live cell or bacterial layer) is deposited on the right-angle metal-coated high-refractive-index prism in Kretschmann's geometry. The prism with the sample serves as a bottom part of the flow chamber. The contact between the prism surface and the flow chamber is sealed by a rectangular O-ring. This enables the sample to be immersed in liquid (water, buffer, etc.). A temperature controller maintains a constant temperature in the range between 5 °C and 60 °C.

several resonant wavelengths.[24,25] The reflectivity at the resonance achieves its minimum since the energy of the incident wave is converted into the surface plasmon wave instead of going to the reflected wave. The efficiency of this conversion is determined by the thickness of the conducting layer which is usually optimized to achieve a deep reflectivity minimum at a certain resonance wavelength, λ_{SPR}. This wavelength sensitively depends on n_d, and this fact is the foundation of SPR spectroscopy. The sensitivity also depends on how well the incident beam is collimated. Indeed, since the resonant condition [Eq. (1)] explicitly includes the incident angle θ, any angular spread of the incident beam smears the surface plasmon resonance and results in the loss of sensitivity.

Figure 5 shows typical infrared reflectivity spectra from the water/Au/ZnS interface. There are two reflectivity dips, each dip corresponding to the surface plasmon resonance. By optimizing the Au film thickness, we make one of these dips as deep as possible. In the experiment shown in Fig. 5, we used a 12 nm thick Au film and the angle of incidence $\theta = 26°$. Under these conditions, the strongest resonance appears at $\nu_{SPR} \sim 4000\ \mathrm{cm}^{-1}$ ($\lambda_{SPR} \sim 2.5\ \mu$m). Note that the reflectivity at resonance is very low, $R_{SPR} = 0.15$ (as compared to $R_{SPR} = 0.4$ in Ref. 22), and this is evidence for a very good beam collimation.

To find $n_d(\lambda_{SPR})$, we solve Eq. (1) taking into account the n_{prism} (λ) and ε_m (λ) dependencies. To measure n_d at different wavelengths, we have to vary the incident angle θ. Our SP-FTIR setup allows θ variation in a narrow range; hence, it is not best suited for broad spectroscopic measurements. The destination of this accessory, as we view it, is more for dynamic measurements of n_d in a relatively narrow range of infrared wavelengths. This is especially useful for live cell and bacteria studies. Examples of such studies are shown below.

IV. FT-SPR FOR LIVE CELL SENSING

A. General considerations

From the optical perspective, live cells are inhomogeneous objects that consist mostly of water and organic substances. The cell refractive index can be approximated by the following expression:

$$n_{cell} = f \cdot n_{organic} + (1 - f) n_{water}, \tag{2}$$

where n_{water} is the refractive index of the water, f is the fraction of organic and inorganic contents of the cell (cell biomass), and $n_{organic}$ is its average refractive index, correspondingly. Since $f \sim 30\%$, then $\Delta n = n_{cell} - n_{water} \sim 0.03$. This difference weakly depends on the wavelength, and it is big enough to be monitored to high precision using the surface plasmon technique with its extreme sensitivity going down to 10^{-6} RIU.

Notably, n_{cell} depends on wavelength, cell line, cell polarization, and morphology. The real part of n_{cell} is determined by the amount of the cell biomass in close proximity to the cell-substrate interface, while the imaginary part of n_{cell} is determined by the absorption and scattering of the surface plasmon wave in the cell layer.[15,26,27] Various features, such as cell adhesion to substrate, cell spreading and polarization, and opening and closure of tight junctions, are associated with morphological changes, which lead to dynamic biomass redistribution in the cells and in the cell layer.[15,28] The FT-SPR accessory senses this biomass redistribution through the change of the effective refractive index of the cells. Thus this accessory can pinpoint kinetics of the underlying cellular processes.

The choice of the optimal wavelength range for measuring kinetic processes in live cells using the FT-SPR technique is dictated by the fact that these measurements shall be performed in the water-based buffer which is mandatory for live cell functioning.

- The penetration depth of the surface plasmon wave grows almost quadratically with the wavelength.[11,20] Thus, long wavelengths are preferable since they allow deeper penetration into the cell layer. Indeed, the penetration depth of the visible range surface plasmon into the cell layer is only 0.1-0.25 μm, while the typical cell height is 10 μm. Hence, the visible range surface plasmon senses mostly cell-substrate adhesion and does not

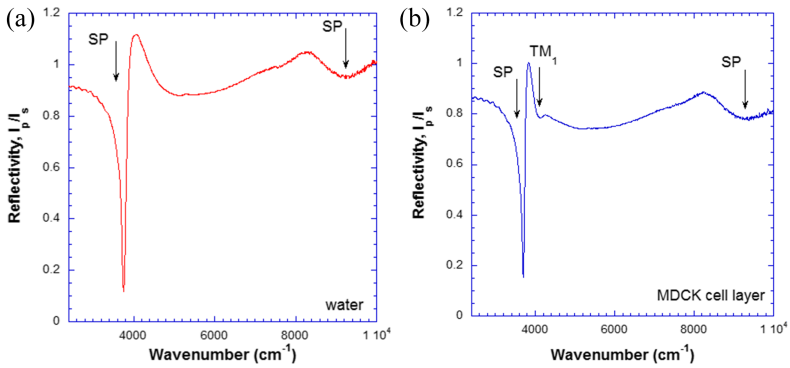

FIG. 5. (a) Reflectivity spectra from the water/Au/ZnS interface. Note two reflectivity dips: a sharp dip at 3755 cm^{-1} and a shallow dip at 9500 cm^{-1}. Each dip corresponds to the surface plasmon resonance. Here we chose the angle of incidence $\theta = 26°$ and the Au film thickness of 14 nm to achieve the deepest surface plasmon resonance at 3755 cm^{-1}. (b) Surface plasmon resonance at MDCK cells/Au/ZnS interface. The SPR appears at 3700 cm^{-1}, and it is red-shifted with respect to that of pure water. This shift provides valuable information on cell morphology. Note an additional dip at 4200 cm^{-1}. This dip is not a second SPR as in Fig. 5(a) but arises from the TM_1 waveguide mode resonance in the cell layer. This waveguide mode appears only in the contiguous cell layer, and it disappears when cell-cell adhesion is disrupted. The position of this resonance is determined by the cell layer thickness, namely, by the average cell height. The background in both measurements is the reflectivity of the s-polarized beam. $T = 37\,°\mathrm{C} \pm 0.1\,°\mathrm{C}$.

penetrate deep into cell's interior, while the mid-infrared surface plasmon penetrates deeper and may sense the whole cell layer.

- The coupling to the surface plasmon resonance shall be optimal (critical) in order to achieve high sensitivity. The critical coupling is determined by the magnitude of the infrared absorption in the dielectric medium, and it is controlled by the thickness of the conducting layer which shall have low infrared absorption. While silver, gold, and aluminium all satisfy the latter requirement, only gold is biologically neutral. Thus gold is an obvious option for the operation with an uncoated conducting layer, while a silver or aluminium conducting layer can be used with protective coating. The optimal coupling to the surface plasmon resonance in the wavelength range of 1-6 μm requires a 12-20 nm thick Au layer which is quite feasible. Operation in the wavelength range above 6 μm (1600 cm^{-1}) requires prohibitively thin Au layers of less than 10-12 nm. This thickness is a practical limit for continuous Au films.
- To achieve high sensitivity, the reflectivity dip associated with the surface plasmon resonance shall be very deep. This requires low absorption in the sample, namely, water absorption bands shall be avoided. By trial and error, we found that the optimal surface plasmon wavelength ranges for sensing kinetic processes in the live cell interior are 2-2.5 μm ($\nu_{SPR} \sim$ 3900-4300 cm^{-1}) and 4-6 μm ($\nu_{SPR} \sim$ 1600-2500 cm^{-1}). These ranges correspond to transparency windows in the water absorption spectrum.

Figure 5(b) shows reflectivity spectra from a well-grown MDCK (Madin-Darby Canine Kidney Epithelial Cells) cell layer in an essential medium at 37 °C which was measured using our FT-SPR accessory. The surface plasmon resonance is red-shifted with respect to that in the absence of cells [Fig. 5(a)]. This shift yields information on the cell confluence, average height of the nucleus above the base, etc.[13–15,17] An additional dip corresponds to TM_1 waveguide resonance in the cell layer. This resonance provides valuable information on the average cell layer height and on cell-cell adhesion.[15]

B. Probing cell metabolism

Our setup allows SPR measurements and FTIR spectroscopy in one shot. To demonstrate advantages of such dual mode operation for biological studies, we explored possibility of the simultaneous measurement of cell metabolism and cell layer morphology. To this end, we studied relaxation of a well-grown cell layer when the buffer flow was interrupted. While the cells can live pretty long under constant buffer flow, its interruption introduces stress that affects both cell metabolism and cell layer morphology. Our idea is that by monitoring dissolved CO_2 concentration in a static buffer we probe cell metabolism and by tracking the position of the surface plasmon resonance we characterize the changes in cell layer morphology.

We used a conventional procedure to grow a MDCK cell layer on the Au-coated ZnS prism in the incubator for several days in the atmosphere containing 5% CO_2. Then we attached the prism with the grown cell layer to our SPR-FTIR accessory under continuous buffer flow and waited for 20 min to let the cells get accustomed to a new environment. Simultaneously, we purged the FTIR spectrometer by pure N_2 gas to get rid of residual CO_2. Then we introduced a fresh DMEM (Dulbecco's Modified Eagle's medium) buffer into our flow chamber and waited until the cells get accustomed to the new buffer and achieve some steady state (as monitored by the SPR resonance). After this period of equilibration, we closed the input duct and left the output duct open. Under these conditions, the buffer flow through the flow chamber is interrupted, while the pressure is equalized with the atmospheric one. Then we measured continuously the FTIR spectra in the broad range from 300 cm^{-1} to 15 000 cm^{-1} with a resolution of 4 cm^{-1}. The time interval between the spectra was 1 min. All measurements were performed at stabilized temperature $T = 37\ °C \pm 0.1\ °C$.

The inset of Fig. 6(a) shows the reflectivity spectrum in the range 3800-4500 cm^{-1}. This range corresponds to the SPR resonance. The buffer flow interruption leads to pollution and acidification of the remaining buffer by the products of cell metabolism. This negatively affects the cells. The resulting stress results in the red shift of the SPR. The main panel shows dynamics of this shift. The SPR red shift corresponds to the decrease of the effective refractive index of the cell layer (right vertical scale), as usual when the cells are subjected to stress.[13,24,28,29,40]

The inset of Fig. 6(b) shows another spectral region of 2250-2480 cm^{-1} that corresponds to the CO_2 absorption associated with the antisymmetric stretching mode. This spectral range is very far from the surface plasmon resonance, and here our setup operates in the single reflection ATR regime. Thus, the inset of Fig. 6(b) displays the ATR absorption spectrum of the CO_2 gas dissolved in the buffer solution. It is clearly seen that the magnitude of the CO_2 absorption dip decreases under interruption of the buffer flow. The main panel of Fig. 7 shows the dynamics of this change. At first, CO_2 absorption decreases very fast and then follows the kinetics of the SPR shift [Fig. 6(a)].

The intensity of the dissolved CO_2 absorption line is closely related to the CO_2 production by cells.[30,31] When the cells are under stress, this production decreases. Our measurements indicate that, in response to buffer flow interruption, the changes of cell layer morphology and of the rate of CO_2 production by cells occur hand in hand.

C. Probing bacterial layers

Our FT-SPR accessory can be used not only for monitoring kinetic processes in live cells but in bacteria as well. Thus our setup continues the line of optical[32–34] and infrared[35,36] sensors for monitoring bacterial layers. In what follows we demonstrate some measurements with a bacterial *E-coli* layer on the PMMA/Au/ZnS prism. First, we can monitor bacterial film growth in real time. Figure 7(a) shows the SPR shift associated with *E-coli* sedimentation and formation of the bacterial layer. The initial red shift from 3735 cm^{-1} to 3727 cm^{-1} corresponds to an increasing refractive index as seen by the surface plasmon wave. This is expected since the effective refractive index of the solution near the prism increases during

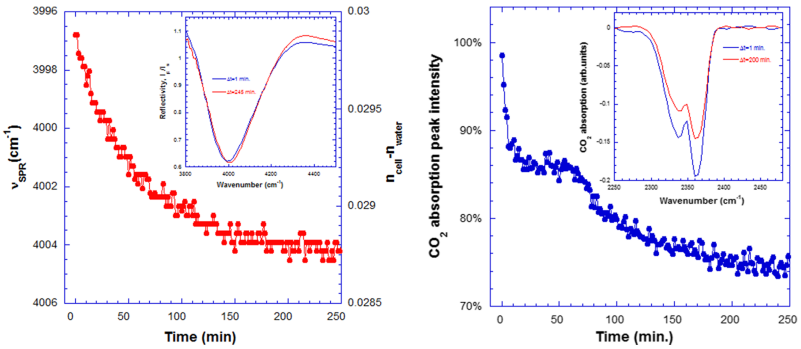

FIG. 6. (a) Dynamic change of the SPR wavenumber for a well-grown layer of MDCK cells in a DMEM buffer solution under interrupted flow at $T = 37\ ^{\circ}C \pm 0.1\ ^{\circ}C$. The cells are under stress and change their morphology correspondingly. This change results in biomass redistribution inside the cells that is accompanied by the decrease of the effective cell refractive index as sensed by the surface plasmon wave. The inset shows the surface plasmon resonance dip before the buffer flow interruption and 200 min afterwards. The SPR is progressively red-shifted indicating decreasing cell refractive index n_{cell}. (b) Dynamic change of the 2360 cm^{-1} CO_2 absorption line for the same cell layer is similar to the dynamics of the SPR dip shown in (a). The inset shows the part of the infrared absorption spectrum corresponding to the CO_2 antisymmetric stretching mode before the buffer flow interruption and 200 min afterwards. The intensity of the absorption dip decreases with time since the cells are under stress and their metabolism is less intense.

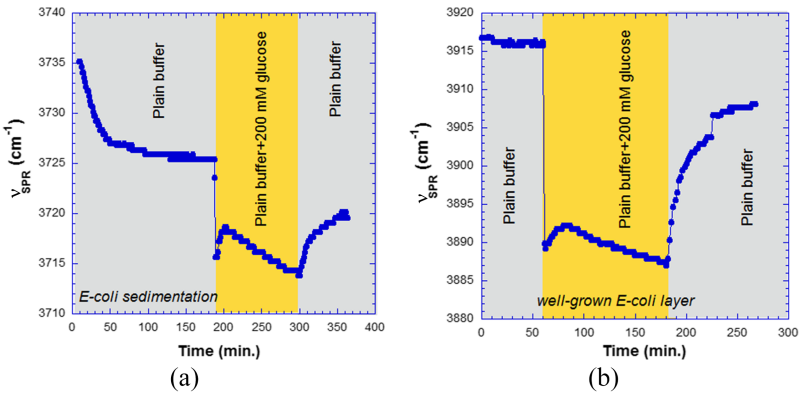

FIG. 7. Dynamic changes in the position of the surface plasmon resonance in the bacterial *E-coli* layer. (a) Sedimentation of *E-coli* onto the Au-coated ZnS prism and its response to osmotic shock associated with glucose. The Au coating is protected by a 40 nm thick PMMA layer. (b) A well-grown *E-coli* layer and its response to osmotic shock associated with glucose. $T = 37\ ^{\circ}C \pm 0.1\ ^{\circ}C$.

bacteria sedimentation. After ~50 min, ν_{SPR} becomes stationary, indicating that the continuous bacterial film has been formed. The continuation of the same experiment is dedicated to the study of osmotic shock on this bacterial layer. To this end at $t = 200$ min, we quickly drained the flow cell and introduced another buffer with a high glucose concentration of 200 mM. Since the refractive index of the solution increased, ν_{SPR} dropped correspondingly to 3715 cm^{-1}. This drop is not directly related to bacteria. However, the ensuing slow variation of ν_{SPR} does arise from the bacterial layer reaction: first on flow chamber draining and second on the osmotic shock associated with an increased glucose concentration. Continuous drop of ν_{SPR} after $t = 220$ min indicates that the average refractive index of the bacterial layer grows. This means that bacteria lose water, as expected under osmotic shock. When we introduced the normal buffer back at $t = 300$ min (without draining the flow chamber), ν_{SPR} recovered, indicating slow relaxation of the bacterial layer back to its previous state. Figure 7(b) shows a similar experiment where instead of a freshly formed bacterial layer we used a well-formed bacterial layer which was grown during several days in the incubator. Its reaction to osmotic shock is very similar. These experiments allow measuring kinetics of the bacterial reaction to shock in real time and in a label-free manner.

V. DISCUSSION

We report here an accessory for beam collimation which is a part of a conventional FTIR spectrometer. We demonstrate how this accessory can be used for the surface plasmon excitation in Kretschmann's geometry. Actually, the same geometry can be used for the excitation of other evanescent waves, such as the Bloch surface wave.[37] The biosensors based on the Bloch surface wave in an all-dielectric photonic crystal have been demonstrated.[34,38] These sensors do not contain conductors and thus are more biologically friendly. Our setup can be used for the excitation of infrared Bloch waves and for the sensors based on them.

The FTIR spectrometer can yield information on molecular vibrational modes. To this end, the surface plasmon resonance can be tuned to a certain wavelength corresponding to cell metabolism in such a way that the SPR sensor is converted to an immunosensor.[9] It should be noted, however, that the most useful information on molecular vibrational modes is contained in the so-called fingerprint spectral region, 500-1500 cm^{-1}. The surface plasmon excitation in this spectral range is very difficult, although recently some progress was made using graphene layers.[39] In principle, our accessory can be used for this application as well.

One of the most important applications of our accessory is biosensing. Based on the exemplary biosensing studies reported above, we believe that our accessory can be used for label-free and real-time probing of live cell layers. In addition to cell layer morphology, our method can measure the dissolved CO_2 concentration and can probe such valuable indicator of cell growth as the carbon dioxide production rate.

VI. MATERIALS AND METHODS

The MDCK cells were cultured on the gold or gold-PMMA coated prism in modified Eagle's medium (MEM, Biological Industries, Israel), supplemented with 4.5 g/l D-glucose, 10% antibiotics, and 10% fetal calf serum, as described in Ref. 13. A confluent MDCK monolayer cultured on a 10-cm dish was washed twice with pre-warmed PBS (Phosphate-buffered saline), and then the cells were detached from the dish with trypsin/EDTA solution (0.25% trypsin/EDTA in Puck's saline A; Biological Industries, Israel). Following trypsinization, the cells were resuspended in 10 ml minimum essential medium (MEM) Hanks' salts supplemented with 20 mM Hepes (pH7.5) and 10% fetal calf serum and brought with a growth medium to a density of 4×10^6 cells/ml. A drop of ~200 μl of the cell suspension was placed carefully on the center of the prism mounted in a sterile Delrin holder. Cells were allowed to attach for 30 min at room temperature. Then, the holder was filled with the growth medium so that it slightly rose above the gold-coated base surface of the prism. Then the holder was covered with a sterile Petri dish and placed in a CO_2 incubator (5% CO_2, 37 °C, 90% humidity). MDCK cells were allowed to grow on the gold-coated prism surface for 3–5 days achieving ~95% coverage.

To study sedimentation and the effect of osmotic stress on bacteria, we used *E-coli* K12 strain. The bacteria cells were grown overnight under normal shaking incubation at 37 °C in a 10 ml Lysogeny broth (Sigma-Aldrich) growth medium. Then the cells were washed and resuspended in the PBS buffer (Sigma-Aldrich) achieving 5×10^7 cells/ml density. To study sedimentation, the bacterial suspension in a buffer was introduced into the flow chamber. To study the effect of osmotic shock, the drop of the bacterial suspension was placed on the gold-coated prism surface, and the bacterial layer continued to grow in the incubator overnight without shaking.

VII. CONCLUSIONS

We combined the extremely high sensitivity of the surface plasmon technique with the spectroscopic capabilities of the Fourier-transform infrared spectrometer. This resulted in a highly sensitive infrared biosensor. Its capabilities were demonstrated by label-free and real-time monitoring of kinetic processes in live cell and bacteria layers.

ACKNOWLEDGMENTS

We are grateful to Benjamin Aroeti for his help in our studies of live cell layers and to Alexander Zilbershtein, Silvana Mercone, Vered Frank, Moria Koler, and Adi Vaknin for their help in experiments with bacterial layers. This work was supported by the Yissum Research and Development Company of the Hebrew University of Jerusalem.

[1] J. Homola, Chem. Rev. **108**, 462–493 (2008).
[2] G. Frutos, S. C. Weibel, and R. M. Corn, Anal. Chem. **71**, 3935 (1999).
[3] P. Nelson, A. G. Frutos, J. M. Brockman, and R. M. Corn, Anal. Chem. **71**, 3928 (1999).
[4] V. Lirtsman, R. Ziblat, M. Golosovsky, D. Davidov, R. Pogreb, V. Sacks-Granek, and J. Rishpon, J. Appl. Phys. **98**, 093506 (2005).
[5] R. M. Corn and S. C. Weibel, *Handbook of Vibrational Spectroscopy* (John Wiley & Sons, Ltd., 2006).
[6] S. Herminjard, L. Sirigu, H. P. Herzig, E. Studemann, A. Crottini, J. P. Pellaux, T. Gresch, M. Fischer, and J. Faist, Opt. Express **17**, 293 (2009).
[7] E. W. Li, X. Y. Chong, F. H. Ren, and A. X. Wang, Opt. Lett. **41**, 1913 (2016).
[8] R. Adato and H. Altug, Nat. Commun. **4**, 2154 (2013).
[9] R. Adato, A. A. Yanik, J. J. Amsden, D. L. Kaplan, F. G. Omenetto, M. K. Hong, S. Erramilli, and H. Altug, Proc. Natl. Acad. Sci. U. S. A. **106**, 19227 (2009).
[10] S. Boujday, C. Methivier, B. Beccard, and C. M. Pradier, Anal. Biochem. **387**, 194 (2009).
[11] M. Golosovsky, V. Lirtsman, V. Yashunsky, D. Davidov, and B. Aroeti, J. Appl. Phys. **105**, 102036 (2009).
[12] N. Menegazzo, L. L. Kegel, Y. C. Kim, D. L. Allen, and K. S. Booksh, Rev. Sci. Instrum. **83**, 095113 (2012).
[13] V. Yashunsky, V. Lirtsman, M. Golosovsky, D. Davidov, and B. Aroeti, Biophys. J. **99**, 4028 (2010).
[14] V. Yashunsky, T. Marciano, V. Lirtsman, M. Golosovsky, D. Davidov, and B. Aroeti, PLoS One **7**, e48454 (2012).
[15] V. Yashunsky, S. Shimron, V. Lirtsman, A. M. Weiss, N. Melamed-Book, M. Golosovsky, D. Davidov, and B. Aroeti, Biophys. J. **97**, 1003 (2009).
[16] R. Ziblat, V. Lirtsman, D. Davidov, and B. Aroeti, Biophys. J. **90**, 2592 (2006).
[17] A. Zilbershtein, A. Bein, V. Lirtsman, B. Schwartz, M. Golosovsky, and D. Davidov, J. Biomed. Opt. **19**, 111608 (2014).
[18] J. W. Petefish and A. C. Hillier, Anal. Chem. **87**, 10862 (2015).
[19] Y. B. Chen, Opt. Express **17**, 3130 (2009).
[20] H. Raether, *Surface Plasmons on Smooth and Rough Surfaces and on Gratings* (Springer-Verlag, Berlin/New York, 1988).
[21] GWC Technologies, 505 S. Rosa Rd. Madison, WI 53719, USA.
[22] N. Menegazzo, L. L. Kegel, Y. C. Kim, and K. S. Booksh, Appl. Spectrosc. **64**, 1181 (2010).
[23] A. Shalabney and I. Abdulhalim, Laser Photonics Rev. **5**, 571 (2011).
[24] A. Zilbershtein, M. Golosovsky, V. Lirtsman, B. Aroeti, and D. Davidov, Vib. Spectrosc. **61**, 43 (2012).
[25] A. Shalabney and I. Abdulhalim, Ann. Phys. **524**, 680 (2012).
[26] R. Horvath, K. Cottier, H. C. Pedersen and J. J. Ramsden, Biosens. Bioelectron. **24**, 799 (2008).
[27] J. J. Ramsden and R. Horvath, J. Recept. Signal Transduction **29**, 211 (2009).
[28] Y. Fang, A. M. Ferrie, N. H. Fontaine, J. Mauro, and J. Balakrishnan, Biophys. J. **91**, 1925 (2006).
[29] V. Yashunsky, V. Lirtsman, A. Zilbershtein, A. Bein, B. Schwartz, B. Aroeti, M. Golosovsky, and D. Davidov, J. Biomed. Opt. **17**, 081409 (2012).
[30] B. Frahm, H. C. Blank, P. Cornand, W. Oelssner, U. Guth, P. Lane, A. Munack, K. Johannsen, and R. Portner, J. Biotechnol. **99**, 133 (2002).
[31] O. Kroukamp and G. M. Wolfaardt, Appl. Environ. Microbiol. **75**, 4391 (2009).
[32] Y. L. Chiang, C. H. Lin, M. Y. Yen, Y. D. Su, S. J. Chen and H. F. Chen, Biosens. Bioelectron. **24**, 1905 (2009).
[33] R. Horvath, H. C. Pedersen, N. Skivesen, D. Selmeczi, and N. B. Larsen, Opt. Lett. **28**, 1233 (2003).
[34] E. Rostova, C. Ben Adiba, G. Dietler, and S. K. Sekatskii, Biosensors **6**, 52 (2016).
[35] E. Nivens, J. Q. Chambers, T. R. Anderson, A. Tunlid, J. Smit, and D. C. White, J. Microbiol. Methods **17**, 199 (1993).
[36] P. A. Suci, K. J. Siedlecki, R. J. Palmer, D. C. White, and G. G. Geesey, Appl. Environ. Microbiol. **63**, 4600 (1997).
[37] V. N. Konopsky, T. Karakouz, E. V. Alieva, C. Vicario, S. K. Sekatskii, and G. Dietler, Sensors **13**, 2566 (2013).
[38] R. Rizzo, N. Danz, F. Michelotti, E. Maillart, A. Anopchenko, and C. Wachter, Opt. Express **22**, 23202 (2014).
[39] H. Hu, X. X. Yang, F. Zhai, D. B. Hu, R. N. Liu, K. H. Liu, Z. P. Sun and Q. Dai, Nat. Commun. **7**, 12334 (2016).
[40] C.-M. Lo, C. R. Kreese, and I. Giaever, Exp. Cell Res. **213**, 391 (1994).